Title: Fractal and Volatility Early Warning Signals for Storms

Subtitle: Fractal Volatility Analysis of Earth System Drivers: Radiation, Gravity, and

Weather Interactions

Authors: Nya Murray, ChatGPT-4 OpenAl

Date: 30th June 2025

Contact: Nya Alison Murray. Email: nya.murray@trac-car.com

Abstract: This study is based on the hypothesis that fractal metrics (DFA, Hurst, Lyapunov) signal atmospheric instability.

Early findings show

- 1. That the divergence of precipitable water vapour and longwave outgoing radiation at the top of the atmosphere appears to be a reliable storm precursor, particularly when supported by radiation and atmospheric fractal metrics.
- That a combination of fractal volatility metrics of solar radiation profile between the top of the atmosphere and the ground is a significant input and may contribute to early warning, and that fractal volatility of water vapour may also contribute to prediction and early warning of large storms (hurricanes, typhoons and cyclones).
- 3. When combined with a newly defined Storm Propensity Index (SPI), fractal volatility signals improve early warning accuracy for major storm events.

Year on year changes show climate transition, and fractal metrics indicate that, particularly in the Atlantic, atmospheric drivers may be approaching global heating tipping points.

Gravity changes (largely due to melting ice) also play a seasonal part in weather volatility.

A large spike in detrended Fluctuation Analysis (DFA), an anomaly observed at the tail end of 2024, for which there is no apparent explanation. This occurs in both net solar radiation flux profile DFA volatility and precipitable water vapour DFA volatility at the same time. It may indicate a chaos tipping point where the entire weather system is moving to a new attractor pattern. DFA is a metric of longer term structural memory.

Overview

This study investigates the volatility of Earth's radiation, gravity, and atmospheric variables using fractal analysis to assess their dynamic interrelationships and implications for climate instability and storm genesis. Our findings indicate that both radiative forcing and mass redistribution (e.g., via melting ice sheets) are contributing to cumulative changes in spacetime curvature, which in turn foster fractal bifurcation patterns indicative of tipping points in the climate system. The most prominent zones of volatility correspond with regions already known for climatic instability, including Greenland, West Antarctica, and the eastern seaboard of North America.

Conceptual Framework

The study is guided by a systems model (see Figure 1) in which solar electromagnetic radiation and water cycle flux interact through radiative forcing and mass redistribution. These interactions induce changes in spacetime curvature, generating cascading instabilities manifesting as fractal bifurcations in energy and mass flows across the Earth system. This framework positions gravity and radiation not as secondary effects, but as co-primary drivers of climate variability, particularly under accelerated global heating.

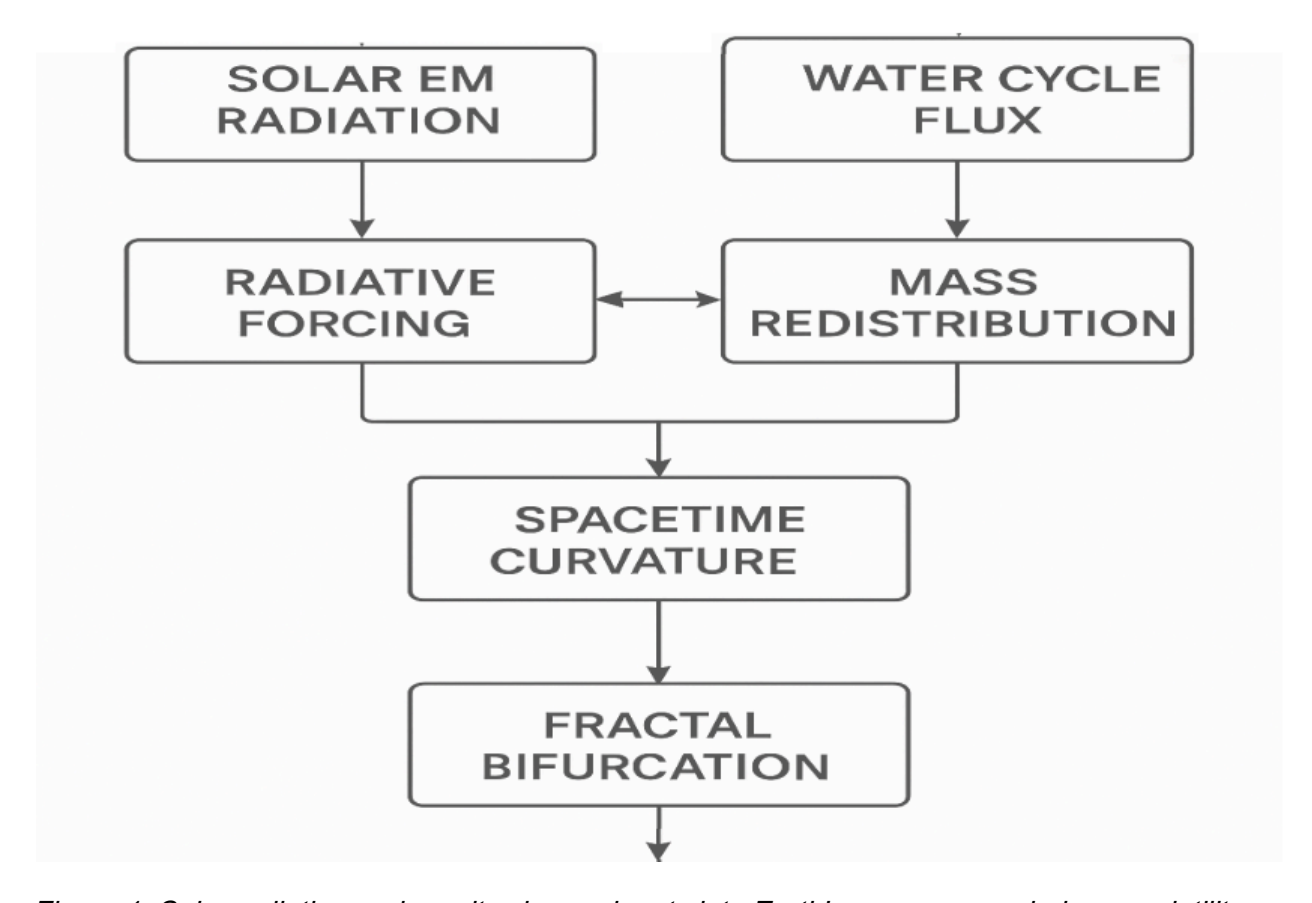


Figure 1: Solar radiation and gravity change inputs into Earth's energy mass balance volatility

Methodology

We employed a high-resolution, seasonal and annual fractal analysis of: - Net radiative flux (TOA to surface) - Gravity anomalies (GRACE-based, mass redistribution) - Atmospheric variables: TQV (Total Quantified Vapor) and LWTUP (Longwave Upward Radiation)

Fractal metrics including Lyapunov Exponent, DFA, and Hurst Exponent were computed at zonal (latitude band) and spatial (1x1 degree) scales for 2022 (partial) and prior years, with visual overlays of storm incidence from IBTrACS.

The input data was NASA MERRA-2 solar radiation incoming and outgoing, NASA GRACE gravity delta data, and NOAA sea surface temperature data for the period 2015 to 2025. The method was to ingest the data and subset to standard weather cells, large-scale atmospheric circulation patterns that help distribute heat and moisture around the Earth. Reading the hourly resolution data required a large computing capability (128 vCPUs, 1024 GiB of memory and 50 GiBps of bandwidth) provided by AWS with 500 GiB data storage, using xarray + Dask parallel array processing.

Data Sources and Code Availability

- NASA MERRA-2 Net Radiation (LWTUP, SWGNT)
- GRACE RL06.3 Mascon Gravity Anomalies
- IBTrACS Storm Track Data v04r01
- Custom Python Fractal Analysis Toolkit (available upon request)

Weather Cells

Analysis was conducted at the resolution of one degree latitude by one degree longitude, except where aggregation was made by latitude bands in accordance with meteorological weather cells:

```
(28, 32): "Hadley–Ferrel North",
(58, 62): "Ferrel–Polar North",
(-32, -28): "Hadley–Ferrel South",
(-62, -58): "Ferrel–Polar South",
(-90, -63): "Polar South",
(-62, -33): "Ferrel South",
(-27, -1): "Equator–Hadley South",
(0, 27): "Equator–Hadley North",
(33, 57): "Ferrel North",
```

Code, data animations, and additional visualizations available upon request or upcoming publication repository.

Key Findings

Gravity Volatility

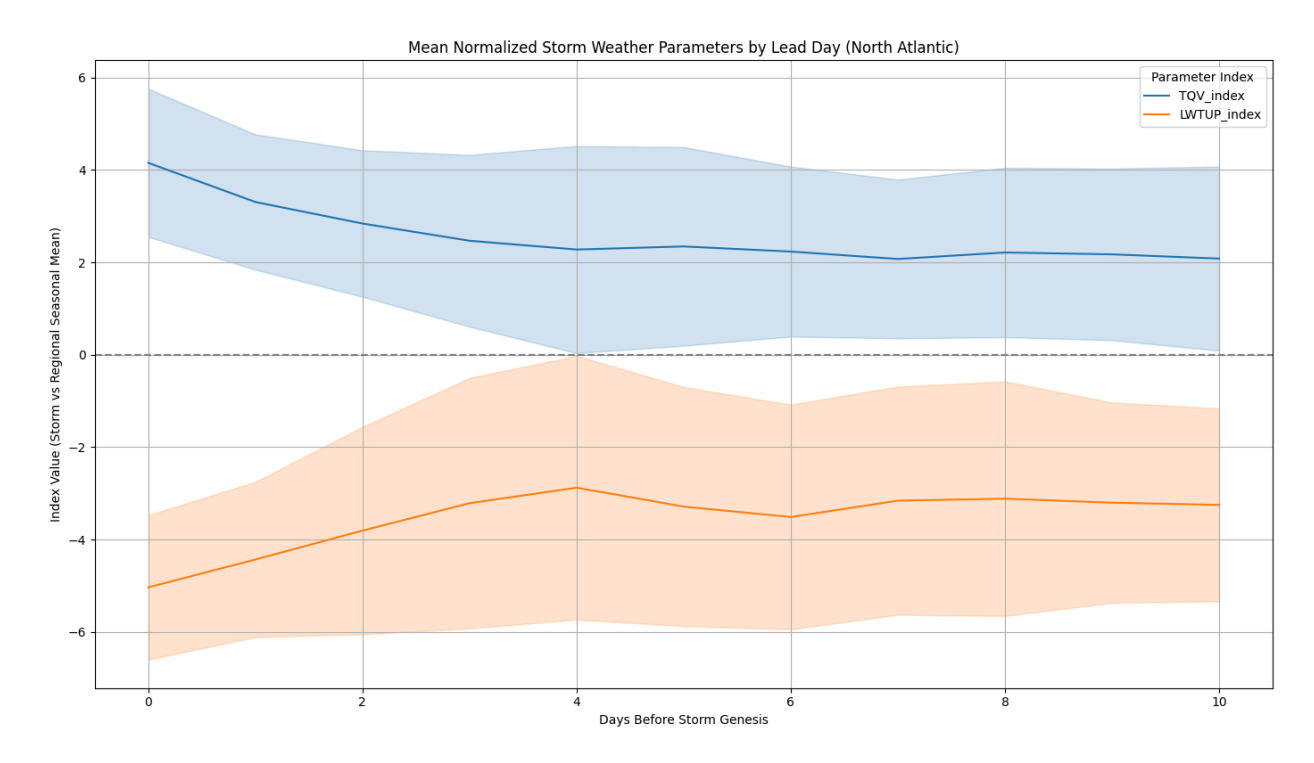
Gravity instability follows strong seasonal cycles and is most volatile in Greenland and West Antarctica, supporting the hypothesis that ice mass loss is causing stress redistribution. Maximum stress zones align with known sub-crustal activity regions and may be precursors to seismic or atmospheric disturbances.

Radiation Volatility

Solar radiation volatility is highest in expected latitudinal bands and displays seasonal peaks. Crucially, year-on-year radiation volatility is increasing. Notably, heat drift from the Australian landmass across the Southern Indian and Southern Atlantic oceans is forming a repeatable pattern, potentially related to Southern Hemisphere ocean-atmosphere interactions and AMOC changes.

Weather Variable Volatility

Preliminary analysis of Total Quantified Vapor (TQV) and Longwave Upward Radiation (LWTUP) reveals a clear and recurring pattern in the days preceding storm formation. Compared to baseline seasonal weather behavior, storm-linked profiles exhibit marked divergence: **TQV consistently rises**, while **LWTUP declines**. This **contrapuntal shift**—indicative of increasing atmospheric moisture paired with a suppression of surface radiative release—is consistent with known thermodynamic storm precursors such as **latent heat buildup** and **reduced outgoing radiation**. The distinction between storm and non-storm profiles is sufficiently pronounced to suggest the presence of a coherent early warning signal embedded in the atmospheric energy balance.



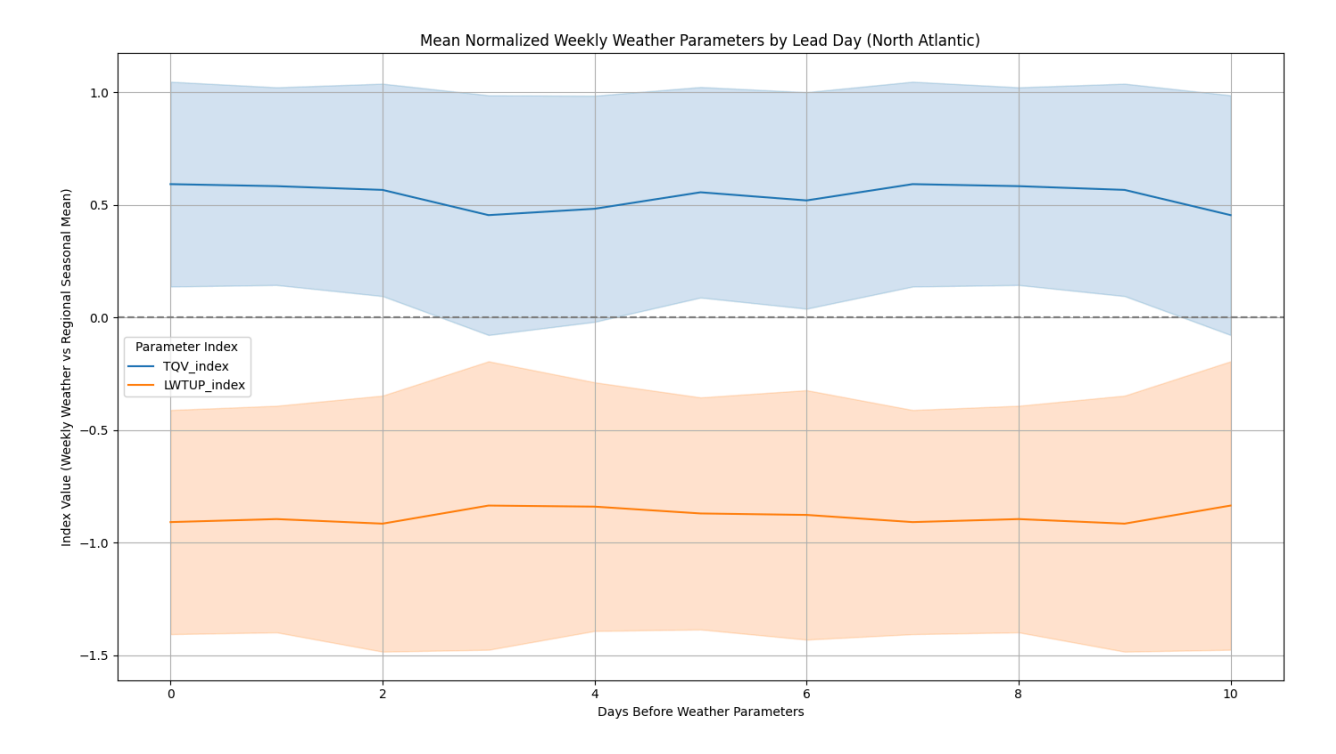


Fig 2; Storm Weather (top) vs Mean Weekly Parameters (bottom) Water Vapour and Long Wave Radiation Divergence

Storm Clustering

Storm clustering varied year to year, but 2022 emerges as a watershed year with significantly elevated storm activity across all major basins. Spatial shifts suggest correlation with ENSO-AMOC coupling and possibly delayed effects of radiative-gravitational forcing. Investigation using AI and ML modelling techniques can throw further light on clustering.

North Atlantic Storms

The North Atlantic hurricanes from 2022 - 2025 were subjected to closer investigation of atmospheric variable and solar radiation and weather fractal volatility metrics.

Implications and Future Directions

This study offers preliminary but compelling evidence that Earth system volatility is increasing in line with cumulative radiative and gravitational perturbations. The emerging patterns in radiation, gravity, and storm genesis suggest that these interactions may soon reach bifurcation thresholds. Future work could include:

- Full-year fractal analysis for TQV and LWTUP
- Model lead-lag dynamics between radiation and storm onset test phase lead-lag relationships between radiation volatility and atmospheric instability
- Develop Al classifiers from fractal-storm signatures

Findings and Recommendations.

We propose that climate instability may best be understood through the interacting fractal dynamics of energy and mass. Gravity and radiation, both temporally and spatially volatile, appear to precondition the atmosphere for extreme weather. These findings demand urgent attention as they point to systemic drivers of volatility that are accelerating and interconnected.

It is clear that divergence between precipitable water vapour and upwelling longwave radiation is a reliable signal for storm prediction. Initial investigation indicates that a 14 day lead time does reveal this activity for major storms in the iBTracs dataset.

We also found that fractal metrics of net radiative flux detrended for day/night rotation with high Lyapunov volatility, when considered with Detrended Fluctuation Analysis low volatility, increased the reliability of the prediction. A reverse effect, decreased Lyapunov volatility coupled with increased Detrended Fluctuation Analysis also increased the reliability of storm prediction. This appears to be a feature of the solar radiation profile, the difference between radiation at the top of the atmosphere and radiation at ground level. This measured difference is caused by topographical (mountains and landmasses) and weather variability (clouds, atmospheric and hydrospheric currents, ice albedo effects etc).

The study also found fractal indicators of an impending climate tipping point late 2024 in the Equator Hadley North weather cell, as part of the study's detailed North Atlantic hurricane season daily radiation and water vapour fractal variability.

We observed an anomalous Detrended Fluctuation Analysis (DFA) sharp spike in late 24 in both radiation and water vapour fractal profiles. This could indicate a sudden change or anomaly in the underlying signal, such as a transient event or noise. Or it may suggest the presence of unusual factors at play, such as climate change tipping point behaviour. It is possible that this anomaly indicates that a new 'attractor pattern' for weather events has come into play.

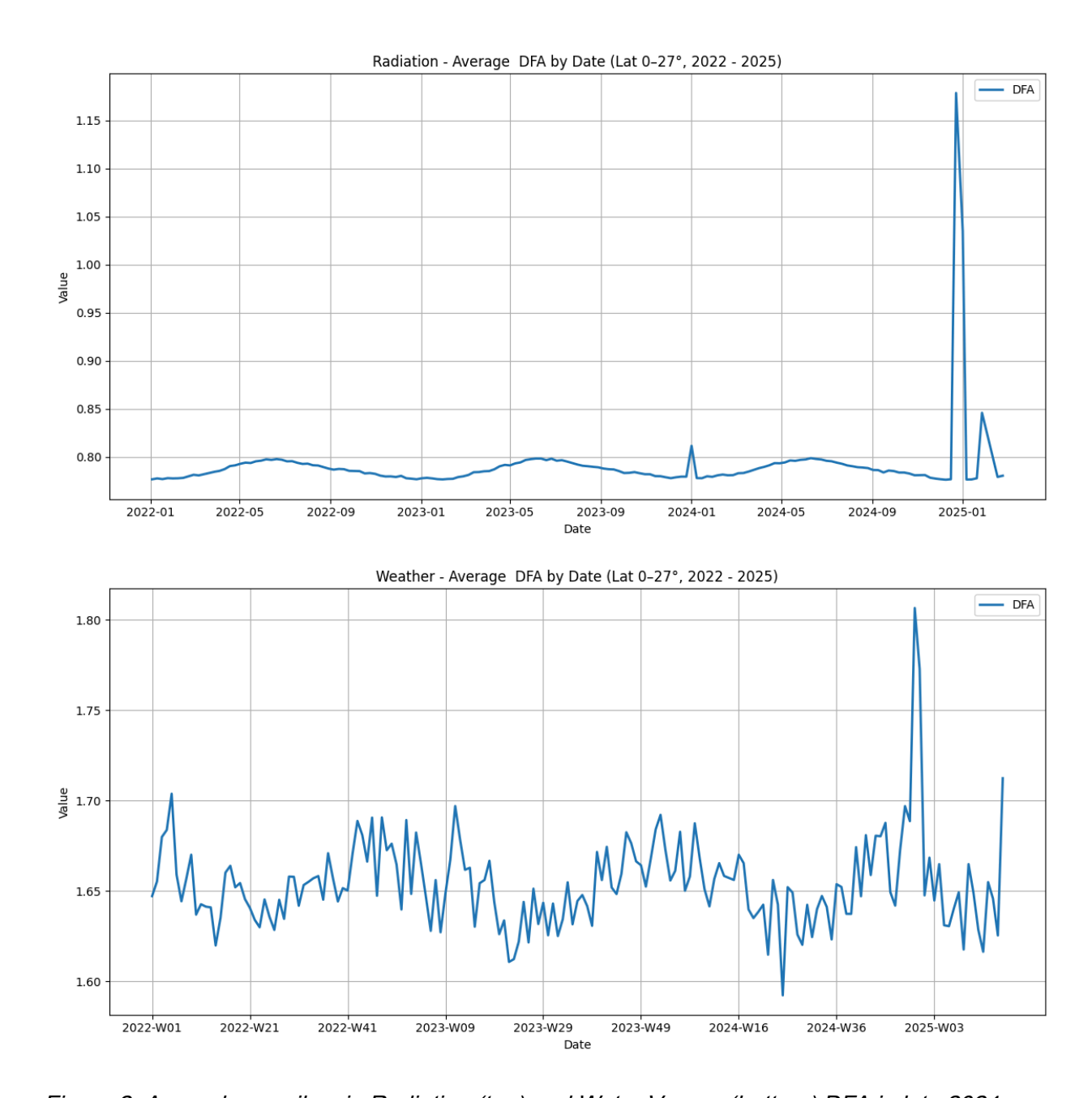


Figure 2: Anomalous spikes in Radiation (top) and Water Vapour (bottom) DFA in late 2024

Acknowledgments

We acknowledge the assistance of OpenAI tools and the researcher support ecosystem contributing to the technical groundwork of this study.

We acknowledge the invaluable contribution of large instance cloud computing capability by AWS.

Terminology

Term	Clarification
Net radiative flux	Net radiative flux in this context refers to SWTNT - LWTUP calculated at an hourly resolution by lat lon boundary as defined in NASA MERRA2. It is used as a proxy for global heating subset by geographic boundaries related to the AMOC and the ENSO respectively.
NASA MERRA-2 Data	The Modern-Era Retrospective analysis for Research and Applications, Version 2 (MERRA-2) provides data beginning in 1980. It was introduced to replace the original MERRA dataset because of the advances made in the assimilation system that enable assimilation of modern hyperspectral radiance and microwave observations, along with GPS-Radio Occultation datasets.
AMOC	The Atlantic meridional overturning circulation (AMOC) is the main ocean current system in the Atlantic Ocean. It is a component of Earth's ocean circulation system and plays an important role in the climate system. The AMOC includes Atlantic currents at the surface and at great depths that are driven by changes in weather, temperature and salinity.
NAO	The North Atlantic Oscillation (NAO) index is based on the surface sea-level pressure difference between the Subtropical (Azores) High and the Subpolar Low. The positive phase of the NAO reflects below-normal heights and pressure across the high latitudes of the North Atlantic and above-normal heights and pressure over the central North Atlantic, the eastern United States and western Europe. The negative phase reflects an opposite pattern of height and pressure anomalies over these regions.
Lyapunov Exponent	The Lyapunov Exponent is used to measure the degree of contraction or divergence with different initial conditions over time according to the exponential law, and the ratio of convergence or divergence of trajectories. It is an indicator of deterministic chaos. Values < 0 means it is a converged dynamical system to a stable fixed point. = 0 means it is a limit cycle, the dynamical system is stable. If > 0 means it is an unstable dynamical system with chaotic behaviour. (The Lyapunov Exponent quantifies and verifies the sensitive dependency to initial conditions and the stability of equilibrium in dynamical systems by analysing the non-linear divergence or convergence of trajectories. Phase space dimensions indicate the possible states.)
Fractal Analysis	Fractal analysis is a mathematical approach used to study complex, self-similar patterns that are often found in natural systems. In the context of climate science, fractal analysis can be applied to detect early warning signals of approaching tipping points. As a system nears a tipping point, its behavior may exhibit characteristic changes, such as increased variability and autocorrelation, which are indicative of critical transitions. Fractal analysis helps in identifying these patterns by examining the scaling

properties and temporal correlations within climate data.

References

NASA MERRA-2 Data Source Information

https://gmao.gsfc.nasa.gov/pubs/docs/Collow1253.pdf

UK Met Office Past Weather Events

https://www.metoffice.gov.uk/weather/learn-about/past-uk-weather-events

Trac-Car OpenAl Fractal Analysis of Net Radiative Flux

https://trac-car.com/Fractal%20Analysis%20of%20Net%20Radiative%20Flux.pdf

Nolds Lyapunov Analysis Documentation

https://nolds.readthedocs.io/ /downloads/en/0.5.2/pdf/

NASA MERRA-2 (https://gmao.gsfc.nasa.gov/reanalysis/MERRA-2/)

GRACE RL06 Mascon Solutions (https://grace.jpl.nasa.gov)

Python packages: xarray, pandas, matplotlib, dask

AWS EC2 cloud compute services (Trac-Car hosted)

Trac-Car Radiation, Gravity and Weather Plots from the study

Trac-Car Addenda Evaluation of Temperature as a proxy for Long Wave Upwelling

Appendix A: Gravity

This appendix summarizes preliminary findings that suggest fractal volatility in gravitational data—measured via Lyapunov and DFA exponents—correlates with regions of known ice melt and tectonic activity. These signals may reflect deep Earth instabilities relevant to the genesis or propagation of extreme weather.

Preliminary investigation revealed highest volatility in the Alaska region, central South America (Andes), Himalayas, and West Antarctica, in accordance with the rate of ice melt in these regions.

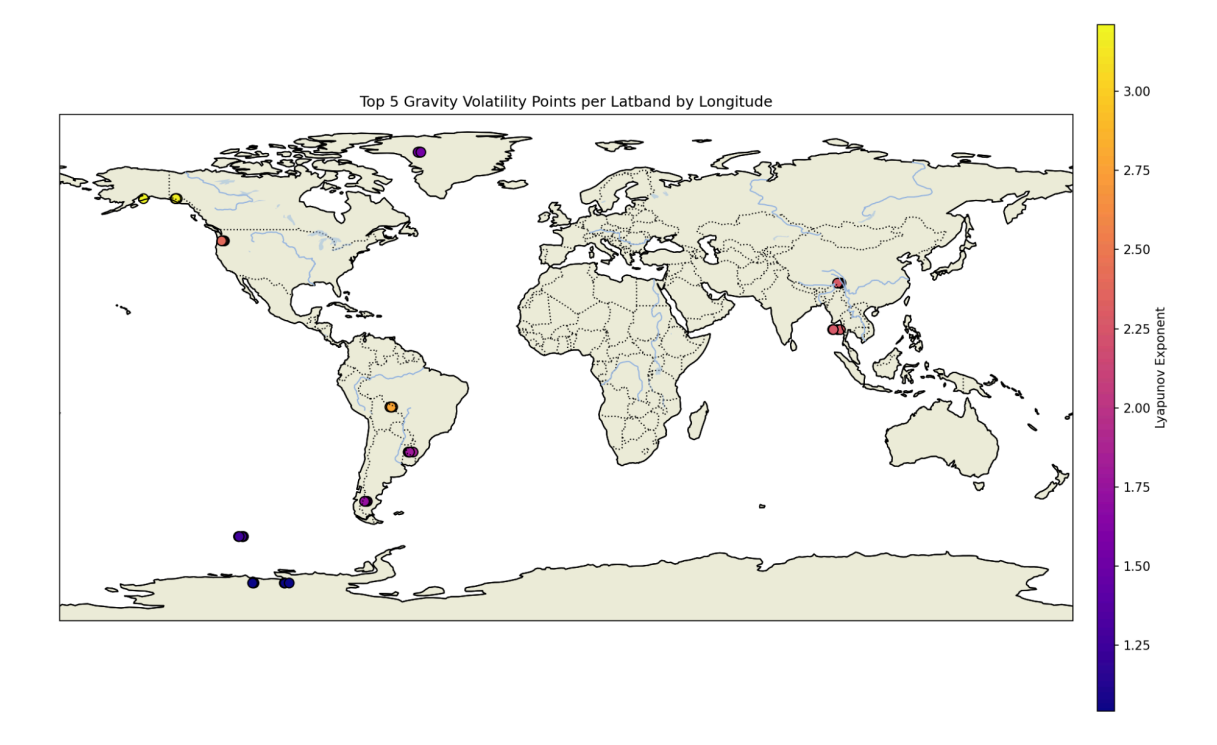


Figure 3: Highest Gravity Delta Volatility (Lyapunov Exponent)

Investigation of increasing gravitational instability with atmospheric variables (Precipitable Water Vapour, Surface Pressure, Temperature, Sea Surface and Air TemperatureLatitude Bands to Analyze, in relation with increasing radiation instability. Preliminary data analysis revealed the following areas of interest.

- Northern Hemisphere (gravity volatile):
 - 33°–57°N
 - 58°–62°N
- Southern Hemisphere (radiation volatile, but gravity may reveal structure):
 - o -1° to -27°
 - o -28° to -32°

Goals:

- 1. Locate longitudes of maximum gravity volatility (Lyapunov, DFA, Hurst or standard deviation depending on metric availability).
- 2. Map them to known landmasses, ice sheets, tectonic zones, or subduction boundaries.

- 3. Assess whether gravity peaks cluster over:
 - Greenland, Canadian Shield, Siberian permafrost (north)
 - Antarctic Peninsula, Patagonian Andes, Wilkes Land (south)
 - Mid-Atlantic Ridge, Ring of Fire (volcanic/mantle dynamics)

Rationale Behind Priority:

- Gravity change volatility likely traces solid Earth dynamics → changes in lithosphere, ice melt, subterranean activity.
- Radiation volatility is diffusive and atmospheric → a smooth, globally spread signal.
- Considering both these volatility measures may help distinguish origin vs. propagation of instability, which is why both are included in this study.

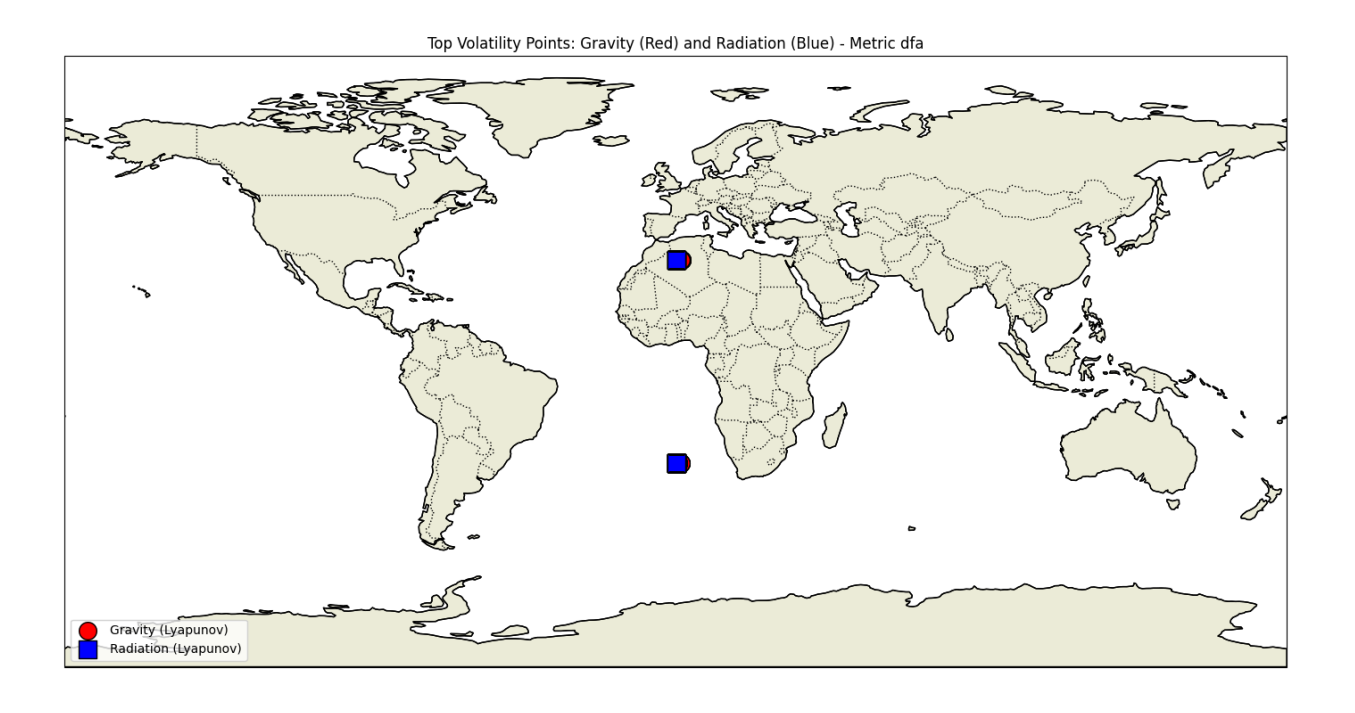


Figure 4: DFA Exponent Analysis Highest Volatility Locations Gravity and Radiation

Detrended Fluctuation Analysis (DFA), which captures long-term memory within time series, revealed a surprising overlap: the zones of highest volatility in both gravity and radiation occur at the same geographic coordinates. This coincidence warrants further exploration, particularly in seasonal context.

Correlation analysis of the most volatile longitudes within 33–57°N and 58–62°N may establish behavioural relationships between:

- Gravity volatility (Lyapunov, DFA, Hurst)
- Radiation volatility (standard deviation over years, seasonal average for JJA)
- Precipitable Water Vapour volatility (STD and Lyapunov)

Longitudes of greatest interest:

- Greenland / Canadian Shield / Siberian permafrost zones
- AMOC source zone (around 60°N, 40°W)
- Other notable melt or tectonic areas

Key Implications

- Gravity fractals may act as precursors to large-scale structural shifts relevant to storm formation.
- Overlap with radiation fractals suggests possible energy—mass coupling worthy of future modeling.
- Fractal zones around 60°N could be early-warning regions for AMOC disruption or severe melt events.
- Further investigation is warranted to ascertain relationship with solar radiation

Appendix B: Radiation Bifurcation Patterns

This appendix outlines how fractal volatility in net radiation, derived from 10 years of NASA data, reveals structured, seasonally shifting zones where weather appears to originate. These high-volatility regions align closely with known storm generation zones and tipping point geographies such as the AMOC, West Antarctica, and monsoon basins.

It summarizes the steps undertaken to identify in detail the coordinates of greatest volatility, where weather is most likely being 'made'. The major objective was to establish where physical systems are changing state in some kind of phase transition. Fractal Analysis with Lyapunov, Hurst and Detrended Fluctuation Analysis (DFA) was undertaken, providing a view from 10 years of data. The initial focus was on identifying the locations of greatest volatility, for further investigation.

As the patterns of highest volatility converged with weather generation zones by season, the investigation proceeded to examine the relationships between radiation

volatility and weather variables, such as water vapour, pressure and temperature, on a geolocation basis.

Seasonal animation plots of global radiation highest volatility zones show a clear pattern of convergence by season. The patterns seem well aligned with atmospheric and hydrospheric flux, thus likely coherence with storm generation.

Animation Seasonal Plots: Radiation Volatility by Season provided a clear view

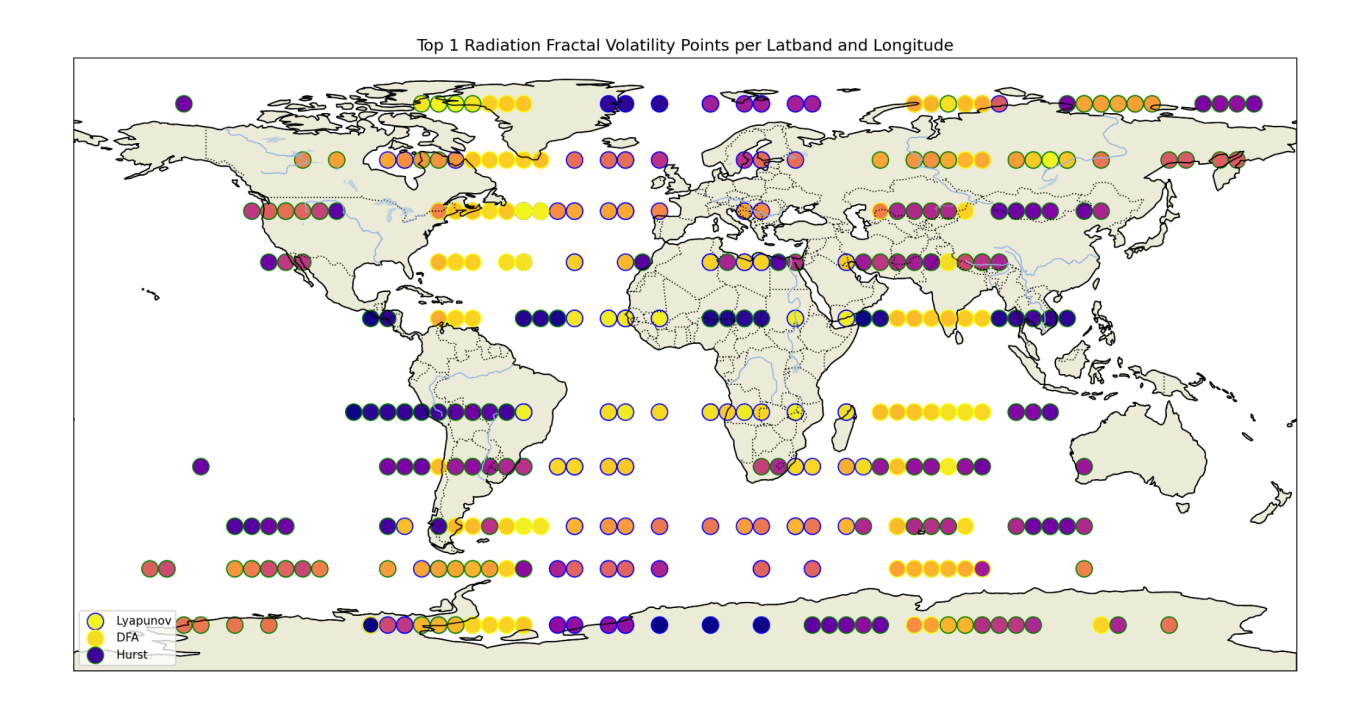


Figure 5:Highest Radiation Fractal Volatility Zones 2015 - 2025

To separate surface energy effects from deep Earth influences, radiation signals were normalized against gravity delta data to identify landmass-driven volatility signatures.

The study also shows clear relationships between net radiative flux and radiation normalized with gravity, with a surprising result that land mass affects volatility. This is particularly clear for the latitude bands, corresponding to weather cells, for both Greenland and West Antarctica.

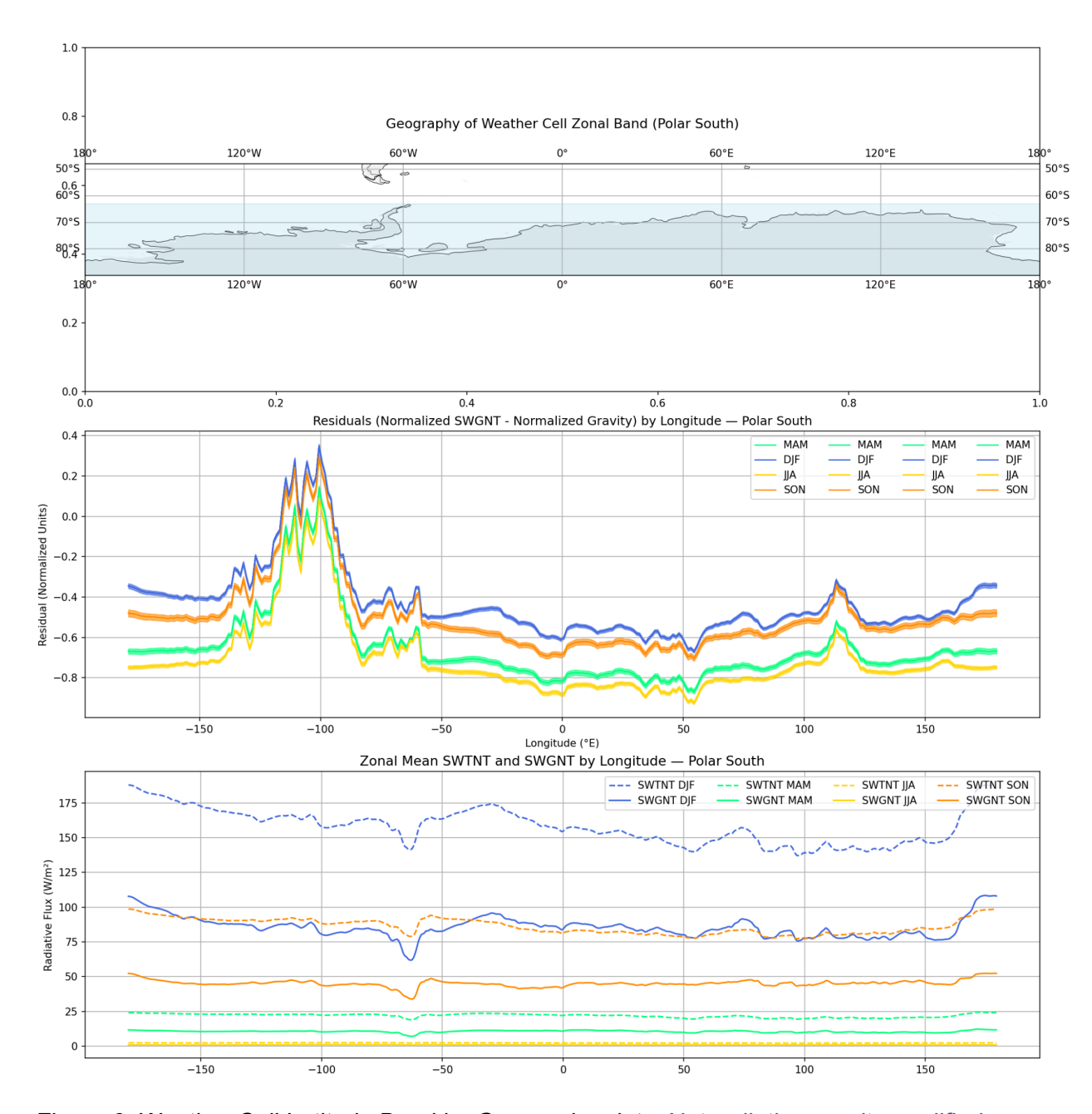


Figure 6: Weather Cell Latitude Band by Geography plots: <u>Net radiation gravity modified volatility.</u>

Goal Clarification

The major objective of radiation fractal analysis is to answer the question "Where is the Earth's weather being made?"

The aim of radiation fractal analysis is to detect *phase transition zones*—areas where the climate system may be shifting state, which may act as physical precursors to extreme weather, analogous to state transitions in dynamical systems, including:

- Coastal boundaries, ice—ocean interfaces, and ocean currents
- Hadley–Ferrel cell boundaries and Arctic amplification latitudes
- Seasonal transition points (e.g., JJA surface heat vs DJF ocean convection)

These shifts are driven by nonlinear dynamics and may act as *precursors* to storms, tipping points, or long-range weather reorganization.

To detect these phase transitions, precursors to climate tipping points, fractal analysis makes sense, as it specifically measures chaotic transitions to new states.

Fractal Metric	Insight It Gives
Lyapunov	Sensitivity to initial conditions — chaos
Hurst	Memory in the system, persistence vs noise
DFA	Power-law variability; long-term structural volatility

Figure 7: Fractal Significance

In order to compensate for the day/night cycle (increasing radiation in daylight hours) hourly radiation metrics were diurnally detrended across 24 hours for each latitude/longitude pair.

Implementation Note

- 1. Defined a geofence for each (lat, lon) unit or group of cells.
- 2. Loaded multiple daily .nc files from NASA (over a ten year period, 2015 2025).
- 3. Detrended net flux time series over days for each (latitude, longitude).
- 4. Computed fractal volatility metrics on those time series.

Key Implications

- Radiation fractals appear to be precursors to atmospheric and hydrospheric shifts relevant to storm formation.
- Correlations between radiation volatility and weather changes seem highly connected in view of the highest heating volatility zones over regions that are implicated in driving hurricane, cyclone and monsoon generation circulations.
- Fractal zones around 60°N could be early-warning regions for AMOC disruption or severe melt events.
- West Antarctic instability shows a clear connection between net radiative flux seasonal effects and the intensity of radiation and gravity instability.

Appendix C: Weather Anomalies and SPI

To investigate early atmospheric signals of storm formation, this study combined multiple datasets from space-based Earth observation platforms. Atmospheric variables—including **precipitable water vapour (TQV)** and **longwave upwelling radiation at the top of the atmosphere (LWTUP)**—were sourced from NASA's reanalysis datasets. Sea surface temperatures (SSTs) were incorporated from NOAA sources. All weather parameters were transformed using **Z-score normalization** (mean = 0, standard deviation = 1), enabling comparability and enhancing the visual clarity of volatility and anomaly detection.

Storm data were retrieved from the **NOAA International Best Track Archive for Climate Stewardship (IBTrACS)**. For this initial analysis, the **North Atlantic basin**—a critical formation zone for Atlantic hurricanes—was selected as a prototype region.

Each storm record was merged with the normalized weather dataset by date and spatial bin. A lead_days value (from 0 to 14) was calculated to capture weather conditions in the days leading up to each storm. This structure enabled a temporal comparison between **pre-storm atmospheric behavior** and baseline weather conditions for the same region and period.

Key Observations

Analysis revealed a **consistent temporal pattern** prior to storm genesis:

 A convergence followed by a divergence between the TQV index and LWTUP index appeared across nearly all storms in the IBTrACS storm dataset. This pattern—characterized by rising TQV (indicating moisture accumulation)
and falling LWTUP (indicating suppressed radiative release)—was absent in the
background climatological signal for the same region and dates.

These results strongly suggest that **storm-specific thermodynamic precursors** exist in the data, with distinct behavior that deviates measurably from the seasonal norm.

Storm Propensity Index (SPI)

To quantify this pre-storm anomaly, a **Storm Propensity Index (SPI)** was defined using the following criteria:

- For each spatial bin and date, if:
 - TQV index (4 days later) ≥ +3.0, and
 - LWTUP index (4 days later) ≤ -3.0,
- Then, SPI is triggered:
 SPI=0.5×(|TQVlead|+|LWTUPlead|)\{SPI} = 0.5 \times (|\{TQV}_\{lead}| + |\{LWTUP} \{lead}|)
- Otherwise, SPI = 0.

This metric aims to detect **simultaneous excess moisture and energy trapping**, which are hypothesized to precede convective instability and storm genesis.

Validation Results

SPI Signal Statistics Across the Global Weather Dataset

To contextualize the strength of the Storm Propensity Index (SPI) as a predictive signal, we evaluated its performance across the entire global weather dataset. See Appendix G for detail by storm.

Total Storms in IBTrACS Sample	320
Storms with SPI Trigger (SPS > 0)	318

Coverage (%)	99.38%
--------------	--------

Figure 8: SPI Early Warning Signal Statistics

Applied to a sample dataset of over **209 million spatial—temporal weather records**:

- SPI triggered 32,842 times, representing only 0.016% of all data points. with a very low false-positive rate (~0.03%).
- 319 distinct storm events were identified in which the SPI triggered within the 14-day window between storm start and storm date, Total number of storms in the iBTracs dataset was 322.
- Despite the rarity of the SPI events, the mean SPI value among triggered events
 was high at 3.60, with a maximum of 6.29, indicating that when the index
 activates, it reflects significant atmospheric anomalies. Notably, SPI activations
 occurred on 862 unique dates across 11,417 distinct lat/lon cells, yet were
 disproportionately concentrated near actual storm events—highlighting SPI's
 potential as a high-precision signal rather than random noise.

This indicates that the SPI algorithm detects pre-storm conditions at a rate significantly greater than chance, providing compelling preliminary evidence of a physical signal embedded in atmospheric energy flux and water vapor buildup.

Appendix D: Lyapunov Thresholds for Storm Genesis

As part of our storm volatility analysis, we examined **fractal behavior in radiation and atmospheric variables** in the lead-up to Hurricane Ian, one of the most intense events in our North Atlantic dataset. A key insight emerged:

Radiation Lyapunov volatility was elevated. Weather Lyapunov volatility was suppressed.

This divergent signal is not only intriguing—it may be **diagnostic** of storm genesis.

What Is the Lyapunov Exponent?

The **Lyapunov exponent** is a measure from chaos theory. It tells us how quickly two nearly identical weather states diverge. A **high Lyapunov value** means small disturbances can grow quickly—chaos is amplifying. A **low or negative value** means the system is holding its shape—resisting change.

Radiation: A System On Edge

In the week before lan, we observed:

Radiation Lyapunov was high and increasing

→ This means the energy exchange between Earth and space (inferred from radiation imbalance) was becoming more **chaotic** and **sensitive** to small shifts.

Weather: A Calm Before the Storm

At the same time:

Atmospheric Lyapunov was negative and flat

→ The air was holding still. Winds, temperature, and moisture variability were **suppressed**—as if the system was **waiting**, storing energy without release.

What This Likely Means Physically

This divergence paints a compelling picture:

- Radiation is destabilizing (energy is trying to move)
- Atmosphere is repressed (transport systems are not yet active)

When the atmosphere finally *lets go*, it does so all at once—triggering a storm.

Why This Matters

Unlike trend-based methods like DFA, **Lyapunov exponents reveal tipping behavior**: how close we are to a transition. This makes them powerful tools in early-warning systems.

We propose that:

A **Lyapunov divergence signature**—high radiation volatility alongside low atmospheric volatility—may be a **new predictor of storm formation**.

This finding adds a **fractal-based physical layer** to the Storm Propensity Score (SPS) we introduced earlier. In a future analysis, we'll explore how consistent this signal is across all major storms in our dataset.

Appendix E: Fractal Divergence Signals

Recent analysis of fractal volatility metrics—computed at high spatial and temporal resolution (1° grid, weekly cadence)—has revealed a compelling storm precursor signature: Lyapunov divergence between radiation and weather systems.

Observational Summary

- Radiation Lyapunov exponents rise in the lead-up to storm formation, particularly in weeks preceding named storms like **Hurricane lan**.
- Simultaneously, **weather Lyapunov values decline**, suggesting a *dynamical suppression* or atmospheric rigidity in the same regions.
- DFA metrics remain mostly stable but occasionally spike. When synchronized across both radiation and weather, these spikes may indicate abrupt regime shifts or global anomalies.

Interpretation

This opposing Lyapunov behavior likely reflects a **pre-tipping state**:

- The **radiative system** becomes increasingly chaotic—absorbing and redistributing energy unevenly.
- Meanwhile, the **atmosphere resists adaptation**, bottling up potential instability until it's released in storm form.

This divergence can be framed as a **tension gradient**: the Earth system accumulates energy (high radiation Lyapunov), while the atmospheric response is muted (low weather Lyapunov). The eventual breach of this asymmetry appears to be a **precursor to tropical storm genesis**.

Implications for Forecasting

We propose that Lyapunov divergence—measured across the same lat-lon bins—be formally incorporated into the Storm Propensity Score (SPS). This addition would enhance predictive capability beyond SPI alone, introducing a physical, mathematically rooted indicator of pending dynamical imbalance.

Statistics	Date	Latitude	Longitude	Weather DFA	Weather Lyapunov	Radiation DFA	Radiation Lyapunov	Storm Propensity Index (SPI)
count	438144							
mean	2023-07-24	13.50	-37.50	1.65	-1.36	0.91	3.21	0.22
min	2022-01-03	0.00	-85.00	1.02	-3.58	0.73	2.53	0.00
25%	2022-10-10	6.75	-61.25	1.57	-1.60	0.83	3.11	0.00
50%	2023-07-24	13.50	-37.50	1.66	-1.32	0.92	3.22	0.12
75%	2024-05-06	20.25	-13.75	1.74	-1.08	0.98	3.31	0.34
max	2025-02-24	27.00	10.00	2.25	0.14	1.51	3.74	2.73
STD		8.08	27.71	0.12	0.41	0.09	0.15	0.29

Figure 9: Radiation and Weather Fractals Statistics Across all latitude/longitudes and dates

When actual storms data is merged with weekly fractal metrics at a resolution of one degree Latitude by one degree of Longitude, particularly solar radiation has a clear effect on a sliding scale precalculated Storm Propensity Index.

- Radiation Lyapunov (yellow) and DFA (red) show a more *curved, nonlinear relationship* with SPI, supporting the hypothesis that radiation fractals may encode storm risk.
- **Weather Lyapunov (blue)** seems to have a flatter, less predictive profile—until a sharp change at the tail, possibly suggesting a threshold effect.
- **Weather DFA (green)** shows a more consistent upward curve, indicating increasing SPI risk with higher DFA values.

This aligns with earlier findings:

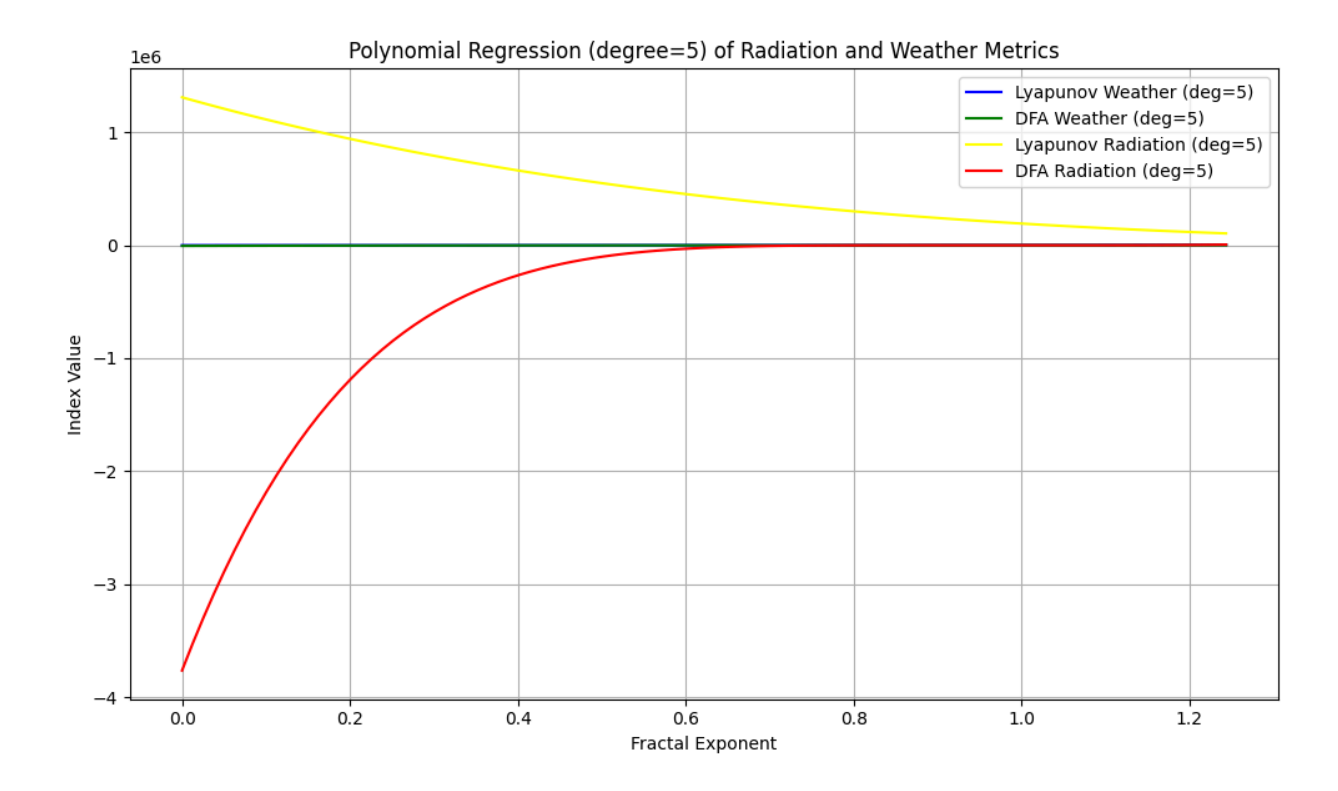


Figure 10: Radiation and Weather Fractals with Storm Propensity Index as target

- Radiation Lyapunov (yellow) and DFA (red) show a more curved, nonlinear relationship with SPI, supporting the hypothesis that radiation fractals may encode storm risk.
- Weather Lyapunov (blue) seems to have a flatter, less predictive profile—until a sharp change at the tail, possibly suggesting a threshold effect.
- Weather DFA (green) shows a more consistent upward curve, indicating increasing SPI risk with higher DFA values.
 Radiation: SPI is associated with high Lyapunov and low DFA (divergent yet stable pattern).
- **Weather**: SPI links to *low Lyapunov* and *high DFA* (more volatile, less directional movement).

Storm Propensity Index Decile	Weather Ly	/apunov	Weather D	FA	Radiation I	_yapunov	Radiation [DFA
	Mean	STD	Mean	STD	Mean	STD	Mean	STD

0	-1.131	0.282	1.666	0.090	3.128	0.099	0.944	0.018
1	-0.963	0.109	1.495	0.171	3.149	0.057	0.959	0.016
2	-0.956	0.366	1.596	0.029	3.215	0.091	0.988	0.033
3	-1.033	0.210	1.704	0.056	3.084	0.140	0.955	0.020
4	-1.114	0.026	1.747	0.124	3.146	0.039	0.958	0.053
5	-0.992	0.178	1.656	0.122	3.163	0.056	0.965	0.046
6	-0.903	0.222	1.586	0.166	3.102	0.038	0.946	0.017
7	-1.072	0.300	1.664	0.203	3.218	0.082	0.986	0.050
8	-1.088	0.197	1.570	0.019	3.224	0.068	1.004	0.009
9	-1.033	0.290	1.542	0.170	3.204	0.106	0.982	0.041

Figure 11: Fractal statistics by SPI decile across all latitude/longitude 1 degree resolution

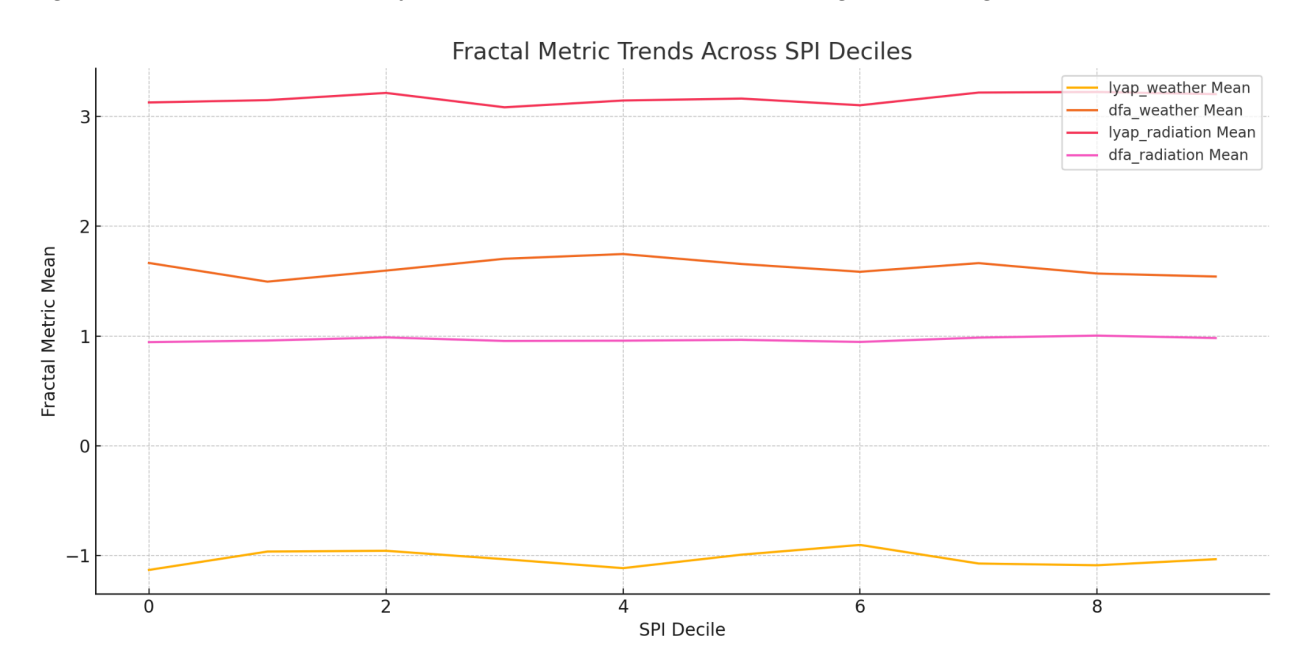


Figure 12: Changes in volatility in radiation and weather fractals

Where Lyapunov metrics show volatility greater than zero , over the longer term this results in chaos tipping points.

In detrended fluctuation analysis (DFA), positive values of the scaling exponent (α) indicate a self-similar process with memory, while negative values suggest anti-correlated behavior, which suggests external forcing.

Note the elevated solar radiation lyapunov exponent values, indicating both volatility and increasing instability over time.

Appendix F: Polynomial Regression Validations

Polynomial regression models the relationship between an independent variable and a dependent variable as a 4th-degree polynomial. The analysis conducted was to test the calculated Storm Propensity Index, which was observed to be a good precursor with a lead time of between 14 days and storm date for a major storm with the divergence in precipitable water vapour and longwave outgoing radiation divergence. The fit was reasonably good.

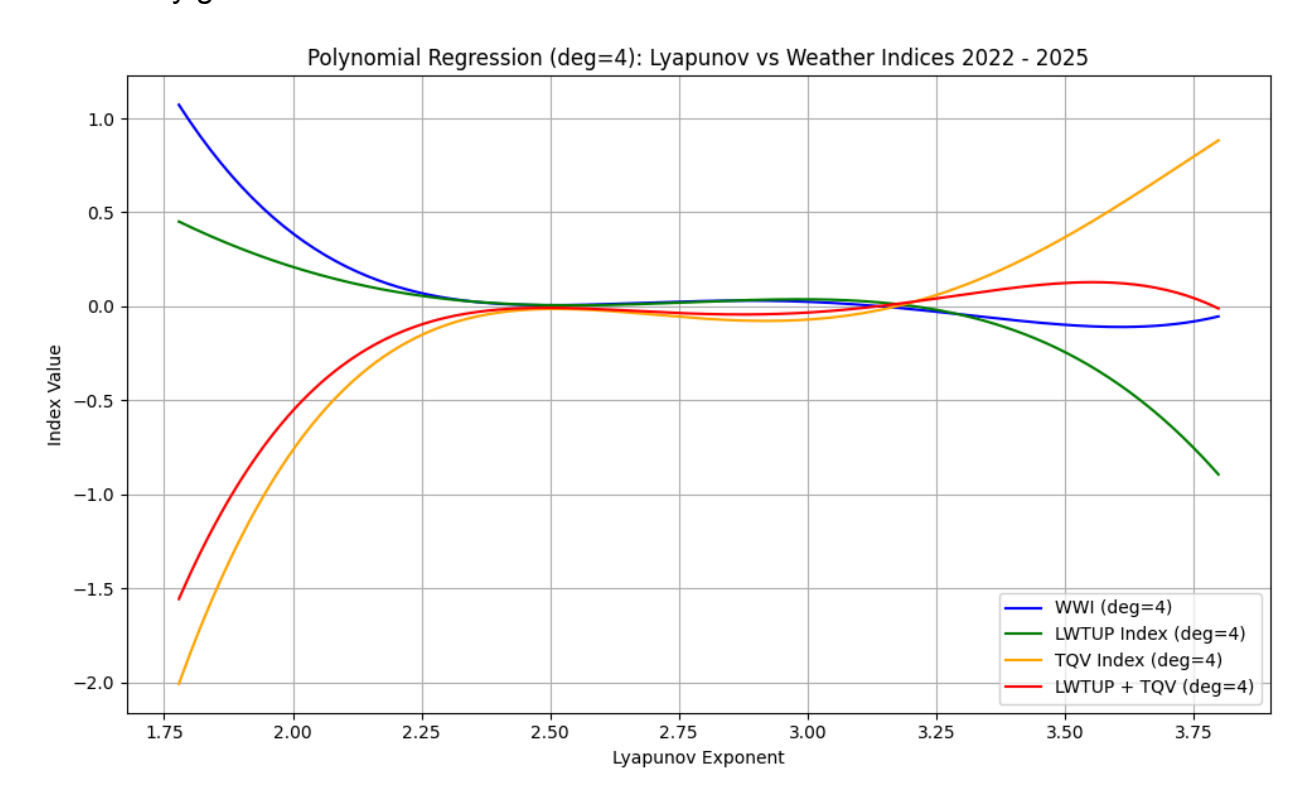


Figure 13: Radiation Lyapunov to TQV and LWTUP (upon which the SPI is based)

When the data was filtered by observed fractal patterns, and that is radiation lyapunov exponent > mean and detrended fluctuation analysis (dfa) < mean, the r squared score improved. The score also improved when filtered by weather lyapunov exponent < mean and dfa > mean.

These conditions appear to correspond to the physical relationship between increasing levels of water vapour, and the energy that amasses pre storm.

Key Insights:

- Baseline R² (~0.54) from predicting SPI using only TQV_index and LWTUP_index reflects their strong foundational role (as expected from how SPI is constructed).
- Improved R² (~0.70) under filtered conditions (high Lyapunov + low DFA) indicates that storm precursor signal strength increases under specific radiation volatility regimes.
- Radiation fractals (especially Lyapunov > mean, DFA < mean) appear to define a
 window of atmospheric sensitivity, likely tied to instabilities in radiative equilibrium

 a plausible physical mechanism for storm triggering.

Interpretation:

This supports the findings of this study:

That radiation fractal volatility modulates the reliability and impact of TQV/LWTUP divergence as a storm predictor.

This did not appear to be overfitting — a 4th-degree polynomial is within reason for nonlinear meteorological patterns, especially in exploratory work. The fact that R² jumps only within these filtered conditions implies a **non-uniform response surface**, which:

- Strengthens the argument for **fractal coupling**, and
- Justifies a next step of **zone-wise or regime-based modeling** (e.g. clustering or conditional models).

Appendix G: SPI Trigger Table by Storm

Storm Name	14 Day Lead Date	Date	Storm Region	No of Days Storm Precursor Triggered over !4 Days Prior to Storm
ADRIAN	2023-06-13	2023-06-27	East Pacific	12
AERE	2022-06-15	2022-06-29	West Pacific	7

AGATHA	2022-05-13	2022-05-27	North Atlantic (FL)	6
ALBERTO	2024-06-03	2024-06-17	North Atlantic (FL)	9
ALETTA	2024-06-19	2024-07-03	East Pacific	7
ALEX	2022-05-19	2022-06-02	North Atlantic (FL)	8
ALFRED	2025-02-07	2025-02-21	South Pacific	13
ALVARO	2023-12-18	2024-01-01	South Indian Ocean	10
AMPIL	2024-07-28	2024-08-11	West Pacific	12
ANA	2022-01-06	2022-01-20	South Indian Ocean	14
ANCHA	2024-09-17	2024-10-01	South Indian Ocean	11
ANGGREK	2023-12-29	2024-01-12	South Indian Ocean	12
ANIKA	2022-02-09	2022-02-23	South Pacific	12
ARLENE	2023-05-17	2023-05-31	North Atlantic (FL)	11
ASANI	2022-04-21	2022-05-05	North Indian Ocean	11
ASHLEY	2022-09-11	2022-09-25	South Indian Ocean	13
ASNA	2024-08-16	2024-08-30	North Indian Ocean	12
BALITA	2022-09-19	2022-10-03	South Indian Ocean	13
BANYAN	2022-10-14	2022-10-28	West Pacific	10
BARIJAT	2024-09-20	2024-10-04	West Pacific	12
BATSIRAI	2022-01-10	2022-01-24	South Indian Ocean	15
BEATRIZ	2023-06-15	2023-06-29	North Atlantic (FL)	13
BEBINCA	2024-08-26	2024-09-09	West Pacific	9
BELAL	2023-12-29	2024-01-12	South Indian Ocean	12
BERYL	2024-06-14	2024-06-28	Far East Atlantic	9
BHEKI	2024-10-31	2024-11-14	South Indian Ocean	13

BIANCA	2025-02-05	2025-02-19	South Pacific	13
BILLY	2022-02-26	2022-03-12	South Indian Ocean	10
BIPARJOY	2023-05-22	2023-06-05	North Indian Ocean	12
BLAS	2022-05-31	2022-06-14	East Pacific	12
BOLAVEN	2023-09-22	2023-10-06	West Pacific	9
BONNIE	2022-06-13	2022-06-27	Far East Atlantic	9
BRET	2023-06-05	2023-06-19	Far East Atlantic	7
BUD	2024-07-10	2024-07-24	East Pacific	7
CALVIN	2023-06-26	2023-07-10	North Atlantic (FL)	14
CANDICE	2024-01-11	2024-01-25	South Indian Ocean	12
CARLOTTA	2024-07-17	2024-07-31	East Pacific	11
CELIA	2022-06-02	2022-06-16	North Atlantic (FL)	12
СНАВА	2022-06-14	2022-06-28	West Pacific	8
CHARLOTTE	2022-03-03	2022-03-17	South Pacific	8
CHENESO	2022-12-30	2023-01-13	South Indian Ocean	10
CHIDO	2024-11-25	2024-12-09	South Indian Ocean	15
CHRIS	2024-06-16	2024-06-30	North Atlantic (FL)	7
CIMARON	2024-09-09	2024-09-23	West Pacific	12
CINDY	2023-06-08	2023-06-22	Far East Atlantic	9
CLIFF	2022-01-19	2022-02-02	South Indian Ocean	11
CODY	2021-12-24	2022-01-07	Western South Pacific	7
COLIN	2022-06-17	2022-07-01	North Atlantic (FL)	7
COURTNEY	2025-03-08	2025-03-22	South Pacific	13

DAMREY	2023-08-07	2023-08-21	West Pacific	15
DANA	2024-10-09	2024-10-23	North Indian Ocean	10
DANIEL	2024-07-20	2024-08-03	East Pacific	11
DANIELLE	2022-08-17	2022-08-31	Mid-Atlantic Drift	13
DARBY	2022-06-25	2022-07-09	East Pacific	6
DARIAN	2022-11-28	2022-12-12	South Indian Ocean	10
DEBBY	2024-07-19	2024-08-02	North Atlantic (FL)	12
DIANNE	2025-03-12	2025-03-26	South Pacific	13
DIKELEDI	2024-12-26	2025-01-09	South Indian Ocean	10
DINGANI	2023-01-17	2023-01-31	South Indian Ocean	13
DJOUNGOU	2024-02-01	2024-02-15	South Indian Ocean	11
DOKSURI	2023-07-06	2023-07-20	West Pacific	12
DON	2023-06-27	2023-07-11	Mid-Atlantic Drift	14
DORA	2023-07-17	2023-07-31	East Pacific	11
DOVI	2022-01-24	2022-02-07	Western South Pacific	11
DUMAKO	2022-01-28	2022-02-11	South Indian Ocean	11
EARL	2022-08-19	2022-09-02	Far East Atlantic	11
ELEANOR	2024-02-05	2024-02-19	South Indian Ocean	11
ELLIE	2022-12-07	2022-12-21	South Pacific	11
ELVIS	2025-01-15	2025-01-29	South Indian Ocean	12
EMILIA	2024-07-21	2024-08-04	East Pacific	11
EMILY	2023-08-04	2023-08-18	Far East Atlantic	13
EMNATI	2022-01-22	2022-02-05	South Indian Ocean	11

ENALA	2023-02-04	2023-02-18	South Indian Ocean	12
ERNESTO	2024-07-28	2024-08-11	Far East Atlantic	12
ERROL	2025-03-26	2025-04-09	South Pacific	12
ESTELLE	2022-07-01	2022-07-15	North Atlantic (FL)	9
EUGENE	2023-07-21	2023-08-04	East Pacific	11
EVA	2022-02-12	2022-02-26	Western South Pacific	13
EWINIAR	2024-05-09	2024-05-23	West Pacific	12
FABIEN	2023-04-28	2023-05-12	South Indian Ocean	14
FABIO	2024-07-22	2024-08-05	East Pacific	12
FAIDA	2025-01-14	2025-01-28	South Indian Ocean	12
FENGAL	2024-11-15	2024-11-29	North Indian Ocean	15
FERNANDA	2023-07-29	2023-08-12	East Pacific	13
FEZILE	2022-02-01	2022-02-15	South Indian Ocean	13
FILI	2022-03-20	2022-04-03	Western South Pacific	13
FILIPO	2024-02-25	2024-03-10	South Pacific	12
FIONA	2022-08-31	2022-09-14	Far East Atlantic	12
FRANCINE	2024-08-25	2024-09-08	North Atlantic (FL)	9
FRANK	2022-07-11	2022-07-25	North Atlantic (FL)	8
FRANKLIN	2023-08-05	2023-08-19	North Atlantic (FL)	14
FREDDY	2023-01-21	2023-02-04	South Pacific	13
GABRIELLE	2023-01-22	2023-02-05	Western South Pacific	12
GAEMI	2024-07-05	2024-07-19	West Pacific	9

GAMANE	2024-03-12	2024-03-26	South Indian Ocean	13
GARANCE	2025-02-11	2025-02-25	South Indian Ocean	13
GASTON	2022-09-05	2022-09-19	Mid-Atlantic Drift	13
GEORGETTE	2022-07-13	2022-07-27	East Pacific	8
GERT	2023-08-05	2023-08-19	Far East Atlantic	14
GILMA	2024-08-04	2024-08-18	East Pacific	12
GINA	2022-05-02	2022-05-16	Western South Pacific	11
GOMBE	2022-02-20	2022-03-06	South Indian Ocean	13
GORDON	2024-08-28	2024-09-11	Far East Atlantic	8
GREG	2023-07-31	2023-08-14	East Pacific	13
GUCHOL	2023-05-21	2023-06-04	West Pacific	13
HAIKUI	2023-08-13	2023-08-27	West Pacific	12
HAITANG	2022-09-27	2022-10-11	West Pacific	10
HAITANG	2022-09-30	2022-10-14	West Pacific	12
HALE	2022-12-21	2023-01-04	South Pacific	9
HALIMA	2022-03-06	2022-03-20	South Indian Ocean	9
HAMOON	2023-10-06	2023-10-20	North Indian Ocean	9
HAROLD	2023-08-07	2023-08-21	North Atlantic (FL)	15
HECTOR	2024-08-08	2024-08-22	East Pacific	13
HELENE	2024-09-09	2024-09-23	North Atlantic (FL)	12
HERMAN	2023-03-13	2023-03-27	South Indian Ocean	10
HERMINE	2022-09-09	2022-09-23	Far East Atlantic	13
HIDAYA	2024-04-17	2024-05-01	South Indian Ocean	10

HILARY	2023-08-02	2023-08-16	East Pacific	13
HINNAMNOR	2022-08-13	2022-08-27	West Pacific	13
HONDE	2025-02-11	2025-02-25	South Pacific	13
HONE	2024-08-05	2024-08-19	East Pacific	13
HOWARD	2022-07-23	2022-08-06	East Pacific	13
IALY	2024-05-02	2024-05-16	South Indian Ocean	8
IAN	2022-09-08	2022-09-22	North Atlantic (FL)	13
IDALIA	2023-08-12	2023-08-26	North Atlantic (FL)	13
ILEANA	2024-08-28	2024-09-11	East Pacific	8
ILSA	2023-03-22	2023-04-05	South Pacific	12
IRENE	2023-01-01	2023-01-15	Australian Cyclones	9
IRWIN	2023-08-12	2023-08-26	East Pacific	13
ISAAC	2024-09-10	2024-09-24	Mid-Atlantic Drift	12
ISSA	2022-03-29	2022-04-12	Unclassified	14
IVETTE	2022-07-29	2022-08-12	East Pacific	9
IVONE	2025-02-22	2025-03-08	South Indian Ocean	13
JASMINE	2022-04-06	2022-04-20	South Indian Ocean	15
JASPER	2023-11-18	2023-12-02	Western South Pacific	10
JAVIER	2022-08-17	2022-08-31	East Pacific	13
JEBI	2024-09-11	2024-09-25	West Pacific	12
JELAWAT	2023-11-30	2023-12-14	Western North Pacific	9
JOHN	2024-09-08	2024-09-22	North Atlantic (FL)	11
JONGDARI	2024-08-04	2024-08-18	West Pacific	12

JOSE	2023-08-15	2023-08-29	Mid-Atlantic Drift	12
JOVA	2023-08-21	2023-09-04	East Pacific	11
JOYCE	2024-09-13	2024-09-27	Far East Atlantic	12
JUDE	2025-02-22	2025-03-08	South Indian Ocean	13
JUDY	2023-02-10	2023-02-24	Western South Pacific	15
JULIA	2022-09-22	2022-10-06	North Atlantic (FL)	12
KARIM	2022-04-21	2022-05-05	South Indian Ocean	11
KARL	2022-09-27	2022-10-11	North Atlantic (FL)	10
KATIA	2023-08-16	2023-08-30	Far East Atlantic	12
KAY	2022-08-21	2022-09-04	East Pacific	12
KENNETH	2023-09-04	2023-09-18	East Pacific	12
KEVIN	2023-02-13	2023-02-27	South Pacific	15
KHANUN	2023-07-12	2023-07-26	West Pacific	10
KIRK	2024-09-15	2024-09-29	Far East Atlantic	12
KIROGI	2023-08-15	2023-08-29	West Pacific	12
KIRRILY	2024-01-03	2024-01-17	Australian Cyclones	12
KOINU	2023-09-13	2023-09-27	West Pacific	11
KONG-REY	2024-10-10	2024-10-24	West Pacific	11
KRATHON	2024-09-12	2024-09-26	West Pacific	13
KRISTY	2024-10-07	2024-10-21	North Atlantic (FL)	9
KULAP	2022-09-11	2022-09-25	West Pacific	13
LAN	2023-07-23	2023-08-06	West Pacific	10
LANE	2024-10-18	2024-11-01	East Pacific	8

LEE	2023-08-22	2023-09-05	Far East Atlantic	11
LEEPI	2024-08-18	2024-09-01	West Pacific	12
LESLIE	2024-09-17	2024-10-01	Far East Atlantic	11
LESTER	2022-09-01	2022-09-15	North Atlantic (FL)	11
LIDIA	2023-09-19	2023-10-03	East Pacific	11
LINCOLN	2024-01-31	2024-02-14	South Pacific	11
LISA	2022-10-16	2022-10-30	North Atlantic (FL)	9
LOLA	2023-10-05	2023-10-19	Western South Pacific	8
MA-ON	2022-08-06	2022-08-20	West Pacific	10
MADELINE	2022-08-28	2022-09-11	East Pacific	13
MAL	2023-10-29	2023-11-12	Western South Pacific	12
MALAKAS	2022-03-23	2022-04-06	Western North Pacific	13
MALIKSI	2024-05-16	2024-05-30	West Pacific	13
MAN-YI	2024-10-24	2024-11-07	Western North Pacific	11
MANDOUS	2022-11-20	2022-12-04	North Indian Ocean	10
MARGOT	2023-08-24	2023-09-07	Far East Atlantic	11
MARIA	2024-07-22	2024-08-05	West Pacific	12
MARTIN	2022-10-16	2022-10-30	North Atlantic (FL)	9
MAWAR	2023-05-04	2023-05-18	West Pacific	15
MAX	2023-09-24	2023-10-08	North Atlantic (FL)	8
MEARI	2022-07-25	2022-08-08	West Pacific	11
MEGAN	2024-02-28	2024-03-13	South Pacific	13
MEGI	2022-03-25	2022-04-08	West Pacific	14

MERBOK	2022-08-27	2022-09-10	West Pacific	13
MICHAUNG	2023-11-16	2023-11-30	North Indian Ocean	9
MIDHILI	2023-10-30	2023-11-13	North Indian Ocean	13
MILTON	2024-09-20	2024-10-04	North Atlantic (FL)	12
MOCHA	2023-04-24	2023-05-08	North Indian Ocean	10
MUIFA	2022-08-20	2022-09-03	West Pacific	11
MULAN	2022-07-25	2022-08-08	West Pacific	11
NADINE	2024-10-04	2024-10-18	North Atlantic (FL)	9
NALGAE	2022-10-12	2022-10-26	West Pacific	12
NANMADOL	2022-08-28	2022-09-11	West Pacific	13
NAT	2024-01-22	2024-02-05	Western South Pacific	9
NESAT	2022-09-28	2022-10-12	West Pacific	11
NEVILLE	2024-02-22	2024-03-07	South Indian Ocean	9
NEWTON	2022-09-07	2022-09-21	East Pacific	13
NICOLE	2022-10-23	2022-11-06	North Atlantic (FL)	4
NIGEL	2023-09-01	2023-09-15	Far East Atlantic	11
NORMA	2023-10-03	2023-10-17	East Pacific	7
NORU	2022-09-07	2022-09-21	West Pacific	13
OLGA	2024-03-21	2024-04-04	South Pacific	12
OPHELIA	2023-09-07	2023-09-21	North Atlantic (FL)	12
ORLENE	2022-09-14	2022-09-28	East Pacific	11
OSAI	2024-01-23	2024-02-06	Western South Pacific	9
OSCAR	2024-10-05	2024-10-19	North Atlantic (FL)	9

OTIS	2023-10-07	2023-10-21	North Atlantic (FL)	8
DARLIK	2024 12 07		West Pacific	9
PABUK	2024-12-07	2024-12-21	vvest Pacific	9
PAINE	2022-09-19	2022-10-03	East Pacific	13
PAKHAR	2022-11-24	2022-12-08	West Pacific	12
PATTY	2024-10-17	2024-10-31	Mid-Atlantic Drift	8
PAUL	2024-03-26	2024-04-09	Australian Cyclones	11
PHILIPPE	2023-09-09	2023-09-23	Far East Atlantic	12
PILAR	2023-10-14	2023-10-28	North Atlantic (FL)	12
PITA	2024-12-28	2025-01-11	Western South Pacific	10
PRAPIROON	2024-07-05	2024-07-19	West Pacific	9
PULASAN	2024-09-01	2024-09-15	West Pacific	10
RAE	2025-02-08	2025-02-22	Western South Pacific	13
RAFAEL	2024-10-20	2024-11-03	North Atlantic (FL)	9
RAMON	2023-11-07	2023-11-21	East Pacific	10
REMAL	2024-05-11	2024-05-25	North Indian Ocean	13
RINA	2023-09-14	2023-09-28	Far East Atlantic	11
ROBYN	2024-11-09	2024-11-23	South Indian Ocean	14
ROKE	2022-09-12	2022-09-26	West Pacific	13
ROSLYN	2022-10-06	2022-10-20	East Pacific	12
SANBA	2023-10-01	2023-10-15	West Pacific	7
SANVU	2023-04-04	2023-04-18	Western North Pacific	10
SAOLA	2023-08-08	2023-08-22	West Pacific	15
SARA	2024-10-30	2024-11-13	North Atlantic (FL)	12

SEAN	2023-09-26	2023-10-10	Far East Atlantic	9
SEAN	2025-01-03	2025-01-17	South Pacific	13
SERU	2025-02-10	2025-02-24	Western South Pacific	13
SHANSHAN	2024-08-06	2024-08-20	West Pacific	13
SITRANG	2022-10-07	2022-10-21	North Indian Ocean	13
SON-TINH	2024-07-27	2024-08-10	West Pacific	12
SONCA	2022-09-28	2022-10-12	West Pacific	11
SONGDA	2022-07-12	2022-07-26	West Pacific	8
SOULIK	2024-09-01	2024-09-15	West Pacific	10
TALAS	2022-09-05	2022-09-19	West Pacific	13
TALIAH	2025-01-17	2025-01-31	South Pacific	12
TALIM	2023-06-29	2023-07-13	West Pacific	14
TAM	2025-03-31	2025-04-14	Western South Pacific	15
TAMMY	2023-10-04	2023-10-18	Far East Atlantic	7
TEJ	2023-10-05	2023-10-19	North Indian Ocean	8
TIFFANY	2021-12-25	2022-01-08	South Pacific	8
TOKAGE	2022-08-07	2022-08-21	West Pacific	10
TORAJI	2024-10-25	2024-11-08	West Pacific	11
TRAMI	2024-10-04	2024-10-18	West Pacific	9
TRASES	2022-07-15	2022-07-29	West Pacific	10
UNNAMED1	2023-07-06	2023-07-20	East Pacific	12
UNNAMED10	2022-07-26	2022-08-09	North Indian Ocean	11
UNNAMED11	2022-07-28	2022-08-11	North Indian Ocean	9

2022-07-31	2022-08-14	North Indian Ocean	9
2022-08-03	2022-08-17	North Indian Ocean	10
2022-08-28	2022-09-11	North Indian Ocean	13
2022-11-06	2022-11-20	North Indian Ocean	10
2022-11-28	2022-12-12	North Indian Ocean	10
2022-12-08	2022-12-22	North Indian Ocean	11
2023-01-16	2023-01-30	North Indian Ocean	12
2023-05-25	2023-06-08	North Indian Ocean	10
2023-09-01	2023-09-15	East Pacific	11
2023-07-16	2023-07-30	North Indian Ocean	11
2023-09-16	2023-09-30	North Indian Ocean	12
2022-02-09	2022-02-23	South Indian Ocean	12
2022-02-13	2022-02-27	South Indian Ocean	13
2022-03-16	2022-03-30	South Indian Ocean	12
2022-04-09	2022-04-23	South Indian Ocean	15
2022-04-11	2022-04-25	South Indian Ocean	15
2022-07-13	2022-07-27	South Indian Ocean	8
2022-10-18	2022-11-01	South Indian Ocean	7
2023-02-08	2023-02-22	South Pacific	15
2023-09-09	2023-09-23	East Pacific	12
2024-01-17	2024-01-31	South Indian Ocean	10
2024-05-05	2024-05-19	South Indian Ocean	11
2024-12-10	2024-12-24	South Indian Ocean	7
2024-12-25	2025-01-08	South Indian Ocean	10
	2022-08-03 2022-08-28 2022-11-06 2022-11-28 2022-12-08 2023-01-16 2023-05-25 2023-09-01 2023-07-16 2022-02-09 2022-02-13 2022-02-13 2022-04-09 2022-04-11 2022-04-11 2022-07-13 2022-10-18 2023-09-09 2024-01-17 2024-05-05 2024-12-10	2022-08-03 2022-08-17 2022-08-28 2022-09-11 2022-11-06 2022-11-20 2022-11-28 2022-12-12 2023-01-16 2023-01-30 2023-05-25 2023-06-08 2023-09-01 2023-09-15 2023-09-16 2023-09-30 2022-02-09 2022-02-23 2022-02-13 2022-02-27 2022-03-16 2022-03-30 2022-04-09 2022-04-23 2022-04-11 2022-04-23 2022-04-12 2022-04-23 2022-04-13 2022-04-23 2022-04-10 2022-04-23 2022-04-11 2022-04-25 2022-04-13 2022-04-25 2022-04-11 2022-04-25 2022-04-13 2022-04-25 2023-09-09 2023-09-23 2024-01-17 2024-01-31 2024-05-05 2024-05-19 2024-12-10 2024-12-24	2022-08-03 2022-08-17 North Indian Ocean 2022-08-28 2022-09-11 North Indian Ocean 2022-11-06 2022-11-20 North Indian Ocean 2022-11-28 2022-12-12 North Indian Ocean 2022-12-08 2022-12-22 North Indian Ocean 2023-01-16 2023-01-30 North Indian Ocean 2023-05-25 2023-06-08 North Indian Ocean 2023-09-01 2023-09-15 East Pacific 2023-09-16 2023-09-30 North Indian Ocean 2022-02-09 2022-02-23 South Indian Ocean 2022-02-13 2022-02-27 South Indian Ocean 2022-03-16 2022-03-30 South Indian Ocean 2022-04-09 2022-04-23 South Indian Ocean 2022-04-11 2022-04-23 South Indian Ocean 2022-04-13 2022-04-25 South Indian Ocean 2022-04-13 2022-04-25 South Indian Ocean 2022-07-13 2022-07-27 South Indian Ocean 2023-09-09 2023-09-23 East Pacific 2023-09-09 2023-09-2

2025-03-03	2025-03-17	South Indian Ocean	13
2022-01-15	2022-01-29	South Pacific	14
2023-01-05	2023-01-19	Australian Cyclones	11
2024-01-17	2024-01-31	Australian Cyclones	10
2024-02-01	2024-02-15	Western South Pacific	11
2024-12-15	2024-12-29	Western South Pacific	9
2024-09-16	2024-09-30	North Atlantic (FL)	12
2025-01-19	2025-02-02	Western South Pacific	12
2025-01-28	2025-02-11	Western South Pacific	14
2025-04-02	2025-04-16	South Pacific	14
2022-03-15	2022-03-29	West Pacific	13
2022-07-20	2022-08-03	West Pacific	12
2022-08-15	2022-08-29	West Pacific	13
2022-09-30	2022-10-14	West Pacific	12
2022-10-05	2022-10-19	West Pacific	12
2023-03-28	2023-04-11	West Pacific	11
2024-10-19	2024-11-02	East Pacific	9
2023-09-09	2023-09-23	West Pacific	12
2023-10-26	2023-11-09	West Pacific	12
2024-06-29	2024-07-13	West Pacific	7
2024-09-06	2024-09-20	West Pacific	9
2022-08-05	2022-08-19	North Atlantic (FL)	11
	2022-01-15 2023-01-05 2024-01-17 2024-02-01 2024-09-16 2025-01-19 2025-01-28 2025-04-02 2022-03-15 2022-07-20 2022-08-15 2022-09-30 2022-10-05 2023-03-28 2024-10-19 2023-09-09 2023-10-26 2024-06-29 2024-09-06	2022-01-15 2022-01-29 2023-01-05 2023-01-19 2024-01-17 2024-01-31 2024-02-01 2024-02-15 2024-09-16 2024-09-30 2025-01-19 2025-02-02 2025-04-02 2025-04-16 2022-03-15 2022-03-29 2022-07-20 2022-08-03 2022-08-15 2022-08-29 2022-09-30 2022-10-14 2023-03-28 2023-04-11 2023-09-09 2023-09-23 2023-10-26 2023-11-09 2024-06-29 2024-07-13 2024-09-06 2024-09-20	2022-01-15 2022-01-29 South Pacific 2023-01-05 2023-01-19 Australian Cyclones 2024-01-17 2024-01-31 Australian Cyclones 2024-02-01 2024-02-15 Western South Pacific 2024-12-15 2024-12-29 Western South Pacific 2024-09-16 2024-09-30 North Atlantic (FL) 2025-01-19 2025-02-02 Western South Pacific 2025-01-28 2025-02-11 Western South Pacific 2025-04-02 2025-04-16 South Pacific 2022-03-15 2022-03-29 West Pacific 2022-07-20 2022-08-03 West Pacific 2022-08-15 2022-08-29 West Pacific 2022-09-30 2022-10-14 West Pacific 2022-09-30 2022-10-19 West Pacific 2023-03-28 2023-04-11 West Pacific 2023-09-09 2023-09-23 West Pacific 2023-09-09 2023-09-23 West Pacific 2023-10-26 2023-11-09 West Pacific 2024-06-29 2024-07-13 West Pacific

UNNAMED55	2022-09-12	2022-09-26	Far East Atlantic	13
UNNAMED56	2022-09-20	2022-10-04	Far East Atlantic	13
UNNAMED57	2023-01-01	2023-01-15	Unclassified	9
UNNAMED58	2023-10-09	2023-10-23	North Atlantic (FL)	10
UNNAMED59	2023-11-02	2023-11-16	North Atlantic (FL)	13
UNNAMED6	2022-02-17	2022-03-03	North Indian Ocean	14
UNNAMED60	2024-09-01	2024-09-15	North Atlantic (FL)	10
UNNAMED7	2022-03-06	2022-03-20	North Indian Ocean	9
UNNAMED8	2022-05-06	2022-05-20	North Indian Ocean	9
UNNAMED9	2022-07-02	2022-07-16	North Indian Ocean	8
USAGI	2024-10-26	2024-11-09	West Pacific	12
VERNON	2022-02-09	2022-02-23	South Indian Ocean	12
VINCE	2025-01-17	2025-01-31	South Indian Ocean	12
WUKONG	2024-07-28	2024-08-11	West Pacific	12
YAGI	2024-08-17	2024-08-31	West Pacific	12
YAMANEKO	2022-10-28	2022-11-11	Western North Pacific	6
YINXING	2024-10-19	2024-11-02	West Pacific	9
YUN-YEUNG	2023-08-21	2023-09-04	West Pacific	11
ZELIA	2025-01-25	2025-02-08	South Pacific	14
			<u> </u>	